Entanglement transition and suppression of critical phase of thermofield double state in monitored quantum circuit with unitary R matrix gates

Shi-Kang Sun[1, 2, *] and Shu Chen[1, 2, †]

[1]*Beijing National Laboratory for Condensed Matter Physics,*
Institute of Physics, Chinese Academy of Sciences, Beijing 100190, China
[2]*School of Physical Sciences, University of Chinese Academy of Sciences, Beijing 100049, China*
(Dated: March 4, 2025)

We study quantum circuits with gates composed randomly of identity operators, projectors, or a kind of R matrices which satisfy the Yang-Baxter equation and are unitary and dual-unitary. This enables us to translate the quantum circuit into a topological object with distinguished overcrossings and undercrossings. The circuit corresponds to a classical loop model when an overcrossings and undercrossing coincides. The entanglement entropy between the final state and initial state is given by the spanning number of the classical model, and they share the same phase diagram. Whenever an overcrossing and undercrossing differ, the circuit extends beyond the classical model. Considering a specific case with R matrices randomly replaced by swap gates, we demonstrate that the topological effect dominates, and only the area-law phase remains in the thermodynamic limit, regardless of how small the replacement probability is. We also find evidence of an altered phase diagram for non-Clifford cases.

Introduction— Quantum circuits provide a natural platform to study discrete quantum evolution and are widely used in quantum computation. In such circuit models, time evolution is implemented as a sequence of quantum gates, and entanglement is the fundamental resource [1–3] that distinguishes quantum computation from its classical counterpart. One of the most intriguing characteristics of the quantum realm is measurement, which also plays an important role in the circuit. Unitary circuits with measurements are often referred to as hybrid or monitored circuits. Measurements are non-unitary and give rise to novel nonequilibrium phenomena, for example, measurement-induced entanglement transitions [4–6], wherein the competition between unitary dynamics and projective measurements leads to fundamentally distinct entanglement scaling regimes.

In recent years, there have been interesting connections between loop models and monitored circuits of Majorana and free fermion models [7–12]. The entanglement transitions therein are related to transitions of classical statistical models. In this work, we attempt to connect the realms of loop models with crossings [13, 14] with a spin-1/2 circuit containing measurements and unitary R matrix gates, and take a step further to explore the effect of distinguishing different crossings, which is not encoded in the classical model and may contain novel phenomena resulting from topological effects.

Loop models are common in statistical physics. For example, they appear in the computation of the partition function of Ising model. Previous literature has studied the loop models with crossings in detail theoretically, relating them to supersymmetric spin chain, integrable models, and the $O(n)$ σ model [14–16], and numerically by Monte Carlo simulations [17, 18]. Quantum loops are also used to model non-Abelian anyons [19] and topological phases [20]. The building blocks of loop models are
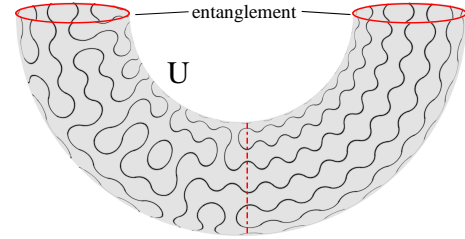

FIG. 1. An illustration of entanglement protocol. U refers to a quantum circuit. The time direction points upward. The part on the right-hand side of central red dashed line depicts an identity evolution of the right part of a thermofield double state $|\Psi\rangle$ (1). The circuit U acts on the left part of $|\Psi\rangle$. We are interested in the entanglement between two parts, indicated by red circles at top.

connecting configurations of "strands" at a lattice site. A similar scenario also appears in integrable vertex systems [21]. Therefore, a natural way to map a loop model to a quantum circuit is to use unitary R matrices [22] from integrable systems as gates of a circuit [23, 24]. R matrices are solutions to the Yang-Baxter equation and also serve as generators of the braid group. They describe braiding of worldlines of particles, which is considered a fault-tolerant method for topological quantum computation with anyons [25]. By allowing unitary R matrix gates, which include simple swap gates as a special case, our circuit is non-orientable [8] and can be always translated to a topological object, which has not been covered in previous studies. They are also dual-unitary [26] and a similar protocol is studied in [27].

Circuit setup and entanglement— In this work we are interested in the entanglement entropy between the initial and final state of a one-dimensional periodic spin 1/2 system, under a monitored quantum circuit with unitary R matrix gates. This differs somewhat from usual entan-

glement entropy defined by a spatial cut of a quantum state and is closer to what is known as pseudo entropy [28] and temporal entanglement [29–32]. It will be more convenient to explore the global (topological) property of the circuit in the following discussion when choosing this definition. We use U to refer to the circuit with forced-measurements, which is a matrix product of unitary gates R, projectors P and identity operators I according to the brickwall pattern, $U = \prod_t \prod_{i=0,1} \otimes_j X^t_{2j-1+i,2j+i}$ where X^t is randomly chosen from R, P and I at time slice t, and the lower index indicates sites that X^t acts on. The probability for unitary gates R is p. At odd time layers the probability for measurement gates P is $(1-p)q$ and the probability for identity gates I is $(1-p)(1-q)$. P and I swap their probability on even time layers. This is the staggered probability setting used in [13] as it respects the $P \leftrightarrow I$ symmetry, which is crucial for the transition therein. Since projector P affects the Frobenius norm of U, $\|U\|_2 := \sqrt{\operatorname{Tr}(U^\dagger U)}$, we define the normalized circuit U' as $U' = U/\|U\|_2$. Then, by singular value decomposition (SVD) $U' = M\Gamma N^\dagger$, we define the entanglement of a single trajectory as $S = -\operatorname{Tr}(\Gamma^2 \log_2 \Gamma^2)$. We are interested in the average entanglement entropy $\langle S \rangle$. This quantity characterizes the extent to which the initial and final state is alike, or how much information about the initial state is lost during the circuit evolution; that is, the more entanglement, the less information loss. We can also characterize the entanglement in an equivalent way by "bending" the initial time boundary to be on the same time-plane as the final time boundary, viewing it as a replica of the original state. An illustration of this protocol is shown in Fig. 1.

In the "bending" picture, the circuit U acts on one side of an infinite-temperature thermofield double state (TFDS)

$$
\begin{aligned}
|\Psi\rangle &= \frac{1}{\sqrt{2^L}} \otimes^L_{i=1} \left(|\uparrow\rangle_i |\uparrow\rangle_{i+L} + |\downarrow\rangle_i |\downarrow\rangle_{i+L} \right) \\
&= \frac{1}{\sqrt{2^L}} \sum_x |x\rangle_1 \otimes |x\rangle_2
\end{aligned}
\tag{1}
$$

where L is system size of either part and $|x\rangle$ is a computational basis. We write subscript 1 and 2 to distinguish two parts. The state $|\Psi\rangle$ can also be referred as a pairing configuration, since every spin at site i is paired with the spin at site $i + L$. A general pairing configuration is written as $|\pi\rangle \propto \otimes_i \left(|\uparrow\rangle_i |\uparrow\rangle_{\pi(i)} + |\downarrow\rangle_i |\downarrow\rangle_{\pi(i)} \right)$.

Intuitively it seems that the entanglement is given by the number of worldlines that connect part 1 and 2. However, this is not always true, as we will see later in this work. But once it is the case, then the entanglement entropy will undergo a transition, which matches the transition of completely packed loop with crossings (CPLC). The transition corresponds to different entanglement scaling with system size averaged from trajectories of time-evolved TFDS $U \otimes I |\Psi\rangle =$

$\sum_i c_i |\Psi_i\rangle_1 \otimes |\Phi_i\rangle_2$. Equivalently, the von Neumann entanglement $S = -\sum_i c_i^2 \log_2(c_i^2)$ between two parts of $|\Psi\rangle$ undergoes a transition.

Building block of the circuit— To build a diagrammatic representation of the circuit, we need to find proper representations for all gates used in the circuit. First, we make R matrix gates generators of a braid group

$$
R := \diagup\!\!\!\!\diagdown , \quad R^\dagger := \diagdown\!\!\!\!\diagup
\tag{2}
$$

and define a Bell state (unnormlized)

$$
|\uparrow\uparrow + \downarrow\downarrow\rangle_{a,b} := \overset{a \quad b}{\smile} , \quad \langle\uparrow\uparrow + \downarrow\downarrow|_{a,b} := \underset{a \quad b}{\frown} ,
\tag{3}
$$

so the (unnormlized) projector and identity operator are

$$
P' := \overset{\frown}{\smile} = |\uparrow\uparrow + \downarrow\downarrow\rangle \langle\uparrow\uparrow + \downarrow\downarrow| , \quad I := \;\Big)\;\Big(.
\tag{4}
$$

P' is not a projector in strict sense since $P'^2 = 2P'$. We interpret the lines in previous diagrammatic representations are worldlines of spins.

In the literature, Kauffman's bracket [33] uses the so-called skein relation to decompose a R matrix as $R = AI + A^{-1}P'$, where A is a free real number. However, this form does not fulfill our purpose because when R is unitary and local dimension $d = 2$, A is limited to $\pm i$. Instead, we introduce a family of unitary R matrices that can be decomposed into three pieces

$$
\begin{aligned}
R &= \frac{1}{\sqrt{\alpha}} \left(a * I + b * P' + c * \operatorname{SWAP} \right) \\
R^\dagger &= \frac{1}{\sqrt{\alpha}} \left(b * I + a * P' + c * \operatorname{SWAP} \right) ,
\end{aligned}
\tag{5}
$$

where SWAP is a swap gate. The swap gate is depicted as a crossing with a dot in the middle, as it does not distinguish an over- or undercrossing:

$$
\operatorname{SWAP} := \diagup\!\!\!\!\!\bullet\!\!\!\!\diagdown .
\tag{6}
$$

In the following we call $P = P'/2$ a projector to simplify notations. We require R matrices to be unitary two-qubit gates and are consistent with topological Reidemeister moves, so they are unitary, dual-unitary and satisfy Yang-Baxter equation $R_{12}R_{23}R_{12} = R_{23}R_{12}R_{23}$, where subscripts indicate the sites the R acting on. Under some algebra, we obtain a one-dimensional parameterization for local dimension $d = 2$: $a = -b = i$, $\alpha = 1 + c^2$ and c is any real number. An explicit matrix representation of R is

$$
R(c) = \frac{1}{\sqrt{\alpha}} \begin{pmatrix} c & 0 & 0 & -i \\ 0 & i & c & 0 \\ 0 & c & i & 0 \\ -i & 0 & 0 & c \end{pmatrix} \xrightarrow{V} \begin{pmatrix} e^{i\phi} & 0 & 0 & 0 \\ 0 & 0 & e^{-i\phi} & 0 \\ 0 & e^{-i\phi} & 0 & 0 \\ 0 & 0 & 0 & e^{i\phi} \end{pmatrix}
\tag{7}
$$

where $\phi = \text{arccot}(c)$ and V is an unitary rotation, $V = e^{i\frac{\pi}{4}X_1}e^{i\frac{\pi}{4}X_2}$. Under the rotation V, R reduces to $e^{-\frac{i\pi}{4}H}$ where H is generally a XXZ hamiltonian, $H = X_1X_2 + Y_1Y_2 - \left(\frac{4}{\pi}\text{arccot}(c) - 1\right)Z_1Z_2 - I$. The X, Y and Z are Pauli operators.

The advantage for taking these R matrices as gates reflects in the topological invariance of worldlines, which means they can be transformed arbitrarily as long as their topology is unchanged. We list some rules for the topology invariant:

$$\bigcirc = n = 2 \ , \quad \text{⤬} = k_+ \bigcup, \quad \text{⤬} = k_- \bigcup \quad (8)$$

where n is loop value, $k_+ = e^{-i\theta}$, $k_- = e^{i\theta}$, $\theta = \arctan(c)$. They are related to the writhe of the corresponding knot. The rules regarding swap gates are:

$$\text{⤬} = \bigcup, \quad \bigcirc\!\!\bullet\!\!(\cdots) = gn^2 \ ,$$
$$\bigcirc\!\!\vdots\!(\cdots) = \bigcirc(\cdots) = n^2 \quad (9)$$

where $g = \frac{k_+ + k_-}{2}$, which simply results from $R + R^\dagger$. This factor will play an important role in discussing the suppression of entanglement. The dashed lines are to indicate different connected components (loops). This relation states that if two distinct loops are stuck together by a dot, the dot will contribute a multiplicative factor g. Given these rules, the topological invariant associated with every closed circuit configuration (periodic in space and time or inner product of two states) can be easily computed. In [34] we show how to compute the invariant of the simplest link, the Hopf link.

Note that in order to make worldlines continuous, all measurements are forced measurements. That is to say, the state after a measurement is just $|\psi'\rangle = P|\psi\rangle$ (without renormalization). To make the mapping between graphical representation and quantum mechanics consistent, we must introduce an additional factor for the inner product of quantum states. In other words, the topological invariant of the worldline braiding of size L equals to $n^{\frac{L}{2}+\#(P)}$ times the inner product of quantum states,

$$n^{\frac{L}{2}+\#(P)}\langle\Psi|\Phi\rangle = \tau(\Psi, \Phi) \ , \quad (10)$$

where $\#(P)$ is the number of measurements in the circuit and τ is the topological invariant of the knot formed by concatenating two pieces of worldline configurations represented by $\langle\Psi|$ and $|\Phi\rangle$.

Effect of links— The main point of this work is to examine the entanglement scaling behavior in the R matrix circuit. To see the relation with CPLC and the importance of the topological effect, let us start from analyzing a very common structure in the circuit, a link. We can check how much von Neumann entropy can be produced by a link of worldlines by computing the entropy of a
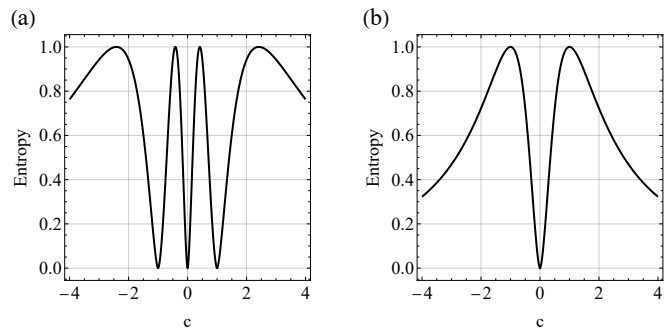

FIG. 2. Entropy produced by a link of worldlines. (a) Link composed by two R matrix gates (11a). The von Neumann entropy is zero at Clifford points and nonzero otherwise. (b) Link composed by one R matrix gate and one swap gate (11b). The von Neumann entropy is not zero at $c = \pm 1$ compared to (a), as a result of different topology. Horizontal: parameter c of R (7).

small circuit piece (11a)

$$(a) \ \text{⤬} \ , \quad (b) \ \text{⤬} \quad (11)$$

and the result is shown in Fig. 2(a). As expected, the von Neumann entropy is zero at Clifford points $c = 0$, $c = \pm 1$ and $\|c\| \to \infty$, where the circuit becomes a Clifford circuit, and nonzero otherwise. For Clifford cases, the entropy is thus given by the spanning number since a crossing does not preserve any entanglement, where the spanning number is defined as the number of worldlines that connect initial and final time boundary. In this setting, a projective measurement acts as an annihilation and creation of a worldline pair, and it can never increase the spanning number. If a measurement annihilates a worldline pair that originally contributes to the spanning number, the entanglement entropy also decreases by 2.

For non-Clifford cases, we anticipate there will be more phases because the entanglement now not only depends on the spanning number but also on concrete link structure inside the circuit. This comes from the topological effect of distinguishing an over- and undercrossing. The entanglement will now be given by the combination of the spanning number and the least number of crossings that must be "cut" to generate a path that winds around whole space. However, it is very hard to directly simulate non-Clifford cases because of the exponential growth of entanglement inside the circuit via tensor network. Fortunately, if one is allowed to replace a $R(c = 1)$ matrix gate by a swap gate randomly, which corresponds to the $\|c\| \to \infty$ case, we may reveal the topological effect and are still able to use the Clifford circuit method. For example, if some circuit pieces becomes (11b) then the entanglement associated with it is shown in Fig. 2(b).

Mapping to CPLC at Clifford points— In the following, we restrict the circuit having a fixed aspect ratio
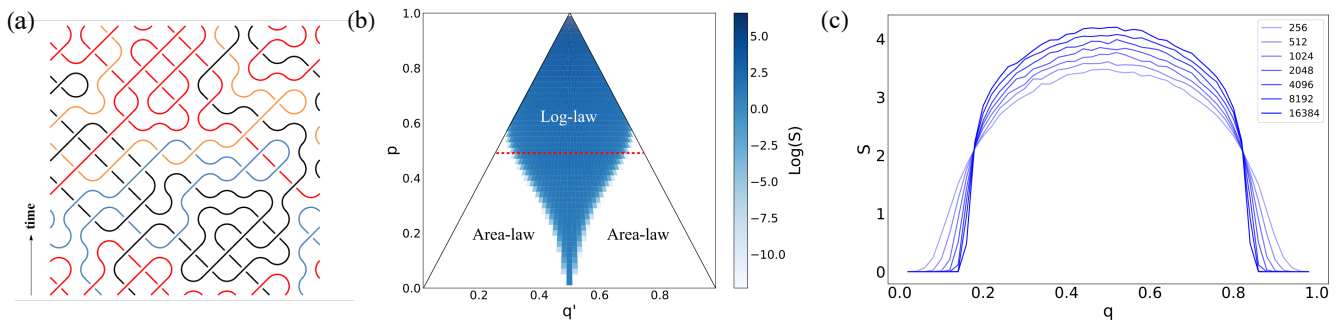
FIG. 3. (a) (Color online) A worldline configuration of loops with crossings that has alternating probability for the projector and identity. Red: worldlines that have both ends on the same boundary, but do not entangle with the other boundary. Black: worldlines that connect two boundaries and contribute to the spanning number. Blue and orange: worldlines that are entangled by a link, in comparison to red ones. (b) Phase diagram of the entanglement entropy in log-scale. p is the probability of R. q' is defined by $(q' - 1/2) = (q - 1/2)(1 - p)$ where q is the probability of P on odd time layers. Blue part represents the critical region where entanglement entropy grows logarithmically with system size L and corresponds to the Goldstone phase of CPLC. White parts are area-law regions where entanglement entropy decays to 0 as system size L grows and correspond to two short loop phases of CPLC. Data shown in (b) are computed at system size $L = 2^{11}$ and $t = L$. We average on 10240 samples. The red dashed line corresponds to data shown in (c). (c) Entanglement entropy of different system size when $p = 0.5$.

1, namely $t = L$ without loss of generality. When $R(c)$ is set at Clifford points, there is no difference between an overcrossing and undercrossing. This means different worldlines can pass through each other freely, as long as their endpoints are fixed. The entanglement between the initial and final state depends solely on the spanning number. Since the probabilities of gates are independent from each other and set identical as in CPLC, the statistics of entanglement can be described by an $n = 1$ CPLC, of which the partition function is

$$Z \equiv \sum_c p^{n_R}[(1-p)q]^{n_m}[(1-p)(1-q)]^{n_I} = 1 \quad (12)$$

where p is the unitary evolution rate, q is the control parameter of the measurement rate, n_m is the number of measurements, n_I is the number of identity gates, n_R is the number of R matrix gates and we sum up all configurations. An example of a configuration is shown in Fig. 3(a). The phase transition of CPLC directly translates to the entanglement transition of quantum circuit.

First let us think about what would happen if there were no crossings in the circuit, or in other words, no unitary gates when $p = 0$. In the no-crossing case, the dynamics can be described by the Templey-Lieb algebra. The graphical representation of the circuit is a soup of bubbles that do not overlap. Since the entanglement entropy is given by the spanning number, we may anticipate a percolation transition in the spatial direction, and there will be no connected worldlines between the initial and final state. In this case, there is a zero entanglement phase produced by the percolation transition. By symmetry, the transition happens when projector probability is $q = 0.5$, so only area-law phases exist when $q \neq 0.5$.

Once unitary R gates are added in the circuit, the dynamics is described by the Birman–Murakami–Wenzl

(BMW) algebra [34]. A new critical phase emerges as shown in Fig. 3(b), and it matches the Goldstone phase of CPLC [13, 14], where entanglement grows logarithmically. We plot the entanglement entropy of different system sizes when $p = 0.5$ in Fig. 3(c). Note that the point $p = 1$ corresponds to a pure unitary circuit by R matrix gates and thus retains maximum entanglement [34]. The diagram boundary lines $q = 0, 1$ correspond also to area law phase, but entanglement increases as $p \to 1$.

Suppression of critical phase by topological effect— In the following, we will focus on the case where we replace $R(c = 1)$ matrix gates by swap gates randomly with probability r, depicted by (11b). As shown in Fig. 2(b), the link now preserves some entanglement. The question we want to ask is, how will this replacement affect the phase diagram? Naively, one might suspect an enriched phase diagram because the spanning number is unchanged by the replacements and there is extra entanglement preserved by a link. However, this is not the case. An intuitive way to understand this result is to see a swap gate as a sum of R and $R^\dagger$ gates. The sum leads to a superposition of circuit configurations, which goes beyond the classical picture where the entanglement only rely on single configuration.

In the language of this work, by including swap gates in the circuit, there will be more and more structures associated with swap gates (9) as the system size L grows. Thus on average, the expected number of g factor, which contributes to the topological invariant τ, increases with L. Since we need renormalization to ensure the diagrammatic representation consistent with the quantum state, the loop value n effectively equals to 1. This means τ will decrease because $g = \frac{1}{\sqrt{2}} < 1$. Additionally, we note that the application of U on $|\Psi\rangle$ leads to a naive superposition

based on R matrix decomposition and (10)

$$|\Psi_f\rangle \propto \sum_\pi \langle \pi | \Psi_f \rangle |\pi\rangle \propto \sum_\pi \tau(\pi, \Psi_f) |\pi\rangle \quad , \qquad (13)$$

since either I, P' or the swap gate only changes a pairing configuration to another, and we denote the final state as $|\Psi_f\rangle = U \otimes I |\Psi\rangle$. In other words, the final state is in the space spanned by different pairing configurations, although they are not orthogonal to each other. The coefficients are given by the topological invariant τ, which decreases exponentially. Since the final state is normalized by definition, it must be supported on a growing exponentially large subspace, which means the final state spreads almost over the whole space it can explore as $L \to \infty$. Note that swap gates conserve the parity $\prod_i Z_i$ of a state and projectors project the state into a locally paired state, then according to (13) final state $|\Psi_f\rangle$ should be an even parity state. If parameters p, q are set in critical region, the spanning number is not zero and both parts of $|\Psi_f\rangle$ are correlated, which means both parts can have odd or even parity, as long as the total parity is even. So the final state approaches a sum of odd and even parity states, namely $|\text{even}\rangle \propto \sum |\prod_i^L Z_i = 1\rangle$,

$$|\Psi_f\rangle \to (|\text{odd}\rangle_1 \otimes |\text{odd}\rangle_2 + |\text{even}\rangle_1 \otimes |\text{even}\rangle_2) \quad , \quad (14)$$

of which the entanglement entropy $\langle S \rangle \to 1$ in the thermodynamic limit, as shown in Fig. 4. When the system size L is small, the additional entanglement preserved by links increase the total entropy. But as L becomes larger, the number of g factor accumulates and dominates, leading to the convergence to 1. For comparison, we also show data for $r = 0$, where no replacement is made and entanglement grows continuously.

So after adding some random replacements of swap gates, the logarithmic increment of entanglement is suppressed. The reminiscent of the original critical phase is the final entanglement convergence to 1 in the thermodynamic limit. However, some parts of original area law phase, that are near original transition lines, are altered by the replacements. In those regions, instead of 0, they acquire some entanglement that is approximately 1. Since in those regions the spanning number is 0 in the thermodynamic limit and contributes no entanglement, we conjecture those regions are related to some structures like chained rings that relate the initial and final time boundary, which could lead to an enriched phase or modified phase boundary in non-Clifford cases [34]. In contrast, the remaining parts far away from original phase boundaries are unaltered by the introduction of swap gates, and the converged value of entanglement is 0 because those two boundaries are totally disconnected as we can draw a line to separate them without breaking any worldline. Thus, the final state can be written as $|\Psi_f\rangle \to |\text{even}\rangle \otimes |\text{even}\rangle$. For example, when $p = 0.2$, $q = 0.2$, $r = 0.1$, the averaged entanglement entropy is almost 0 even when $L = 64$.
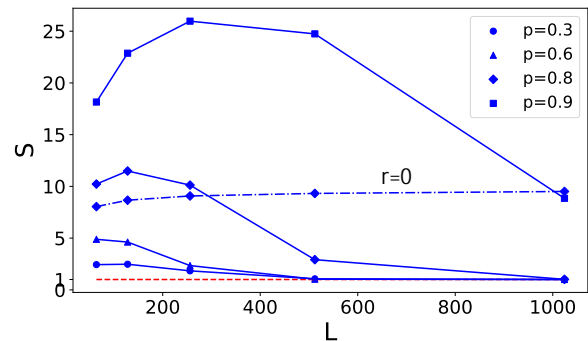

FIG. 4. System size scaling of average entanglement entropy at time $t = L$ for $q = 0.5$, $r = 0.1$, which corresponds to critical region of CPLC. Data shows convergence to $S = 1$. The dash-dot line corresponds to $p = 0.8$, $r = 0$, where no replacement is made. Red dashed line is the reference line for $S = 1$. All data points are averaged from 16384 samples.

Conclusion— In this work, we construct a 4-dimensional matrix representation of the braid group generator, which corresponds to an unitary R matrix family of XXZ model. We study the averaged entanglement between the initial and final state under the circuit evolution made by these R matrices and relevant gates. When the circuit is Clifford the circuit can be described by CPLC and entanglement shares the same phase diagram. However, although the circuit is still Clifford if we replace some R matrix gates by swap gates, the previous phase diagram is completely destroyed as the critical phase is suppressed by a topological effect, in contrast to previous result under general Gaussian unitary gates [9]. The averaged entanglement approaches 1 if in the original critical phase and 0 if in area-law phases that are far away from phase boundaries. The remaining parts, which are in area-law phases but near phase boundaries, also approach 1 for any small amount of random replacements. We conjecture they are evidence that the phase diagram will be enhanced by R matrix gates outside Clifford points, and leave this conjecture to future work.

---

* sunsk@iphy.ac.cn
† schen@iphy.ac.cn

[1] R. Horodecki, P. Horodecki, M. Horodecki, and K. Horodecki, Quantum entanglement, Rev. Mod. Phys. **81**, 865 (2009).

[2] E. Chitambar and G. Gour, Quantum resource theories, Rev. Mod. Phys. **91**, 025001 (2019).

[3] D. Gross, S. T. Flammia, and J. Eisert, Most quantum

states are too entangled to be useful as computational resources, Phys. Rev. Lett. **102**, 190501 (2009).

[4] B. Skinner, J. Ruhman, and A. Nahum, Measurement-induced phase transitions in the dynamics of entanglement, Phys. Rev. X **9**, 031009 (2019).

[5] Y. Li, X. Chen, and M. P. A. Fisher, Measurement-driven entanglement transition in hybrid quantum circuits, Phys. Rev. B **100**, 134306 (2019).

[6] M. P. Fisher, V. Khemani, A. Nahum, and S. Vijay, Random quantum circuits, Annual Review of Condensed Matter Physics **14**, 335 (2023).

[7] A. Nahum and B. Skinner, Entanglement and dynamics of diffusion-annihilation processes with majorana defects, Phys. Rev. Res. **2**, 023288 (2020).

[8] K. Klocke and M. Buchhold, Majorana loop models for measurement-only quantum circuits, Phys. Rev. X **13**, 041028 (2023).

[9] J. Merritt and L. Fidkowski, Entanglement transitions with free fermions, Phys. Rev. B **107**, 064303 (2023).

[10] M. Fava, L. Piroli, T. Swann, D. Bernard, and A. Nahum, Nonlinear sigma models for monitored dynamics of free fermions, Phys. Rev. X **13**, 041045 (2023).

[11] K. Klocke, J. E. Moore, and M. Buchhold, Power-law entanglement and hilbert space fragmentation in nonreciprocal quantum circuits, Phys. Rev. Lett. **133**, 070401 (2024).

[12] K. Klocke, D. Simm, G.-Y. Zhu, S. Trebst, and M. Buchhold, Entanglement dynamics in monitored kitaev circuits: loop models, symmetry classification, and quantum lifshitz scaling (2024), arXiv:2409.02171.

[13] A. Nahum, P. Serna, A. M. Somoza, and M. Ortuño, Loop models with crossings, Phys. Rev. B **87**, 184204 (2013).

[14] J. L. Jacobsen, N. Read, and H. Saleur, Dense loops, supersymmetry, and goldstone phases in two dimensions, Phys. Rev. Lett. **90**, 090601 (2003).

[15] N. Read and H. Saleur, Exact spectra of conformal supersymmetric nonlinear sigma models in two dimensions, Nuclear Physics B **613**, 409 (2001).

[16] M. J. Martins, B. Nienhuis, and R. Rietman, Intersecting loop model as a solvable super spin chain, Phys. Rev. Lett. **81**, 504 (1998).

[17] W. Kager and B. Nienhuis, Monte carlo study of the hull distribution for the q = 1 brauer model, Journal of Statistical Mechanics: Theory and Experiment **2006**, P08004 (2006).

[18] Y. Ikhlef, J. Jacobsen, and H. Saleur, Non-intersection exponents of fully packed trails on the square lattice, Journal of Statistical Mechanics: Theory and Experiment **2007**, P05005 (2007).

[19] P. Fendley, Topological order from quantum loops and nets, Annals of Physics **323**, 3113 (2008).

[20] M. A. Levin and X.-G. Wen, String-net condensation: A physical mechanism for topological phases, Phys. Rev. B **71**, 045110 (2005).

[21] R. J. Baxter, *Exactly Solved Models in Statistical Mechanics* (WORLD SCIENTIFIC, 1985).

[22] H. A. Dye, Unitary solutions to the yang–baxter equation in dimension four, Quantum Information Processing **2**, 117 (2003).

[23] M. Ljubotina, L. Zadnik, and T. Prosen, Ballistic spin transport in a periodically driven integrable quantum system, Phys. Rev. Lett. **122**, 150605 (2019).

[24] L. Sá, P. Ribeiro, and T. Prosen, Integrable nonunitary open quantum circuits, Phys. Rev. B **103**, 115132 (2021).

[25] C. Nayak, S. H. Simon, A. Stern, M. Freedman, and S. Das Sarma, Non-abelian anyons and topological quantum computation, Rev. Mod. Phys. **80**, 1083 (2008).

[26] B. Bertini, P. Kos, and T. Prosen, Exact correlation functions for dual-unitary lattice models in $1 + 1$ dimensions, Phys. Rev. Lett. **123**, 210601 (2019).

[27] M. Ippoliti and V. Khemani, Postselection-free entanglement dynamics via spacetime duality, Phys. Rev. Lett. **126**, 060501 (2021).

[28] Y. Nakata, T. Takayanagi, Y. Taki, K. Tamaoka, and Z. Wei, New holographic generalization of entanglement entropy, Phys. Rev. D **103**, 026005 (2021).

[29] M. B. Hastings and R. Mahajan, Connecting entanglement in time and space: Improving the folding algorithm, Phys. Rev. A **91**, 032306 (2015).

[30] A. Lerose, M. Sonner, and D. A. Abanin, Influence matrix approach to many-body floquet dynamics, Phys. Rev. X **11**, 021040 (2021).

[31] A. Foligno, T. Zhou, and B. Bertini, Temporal entanglement in chaotic quantum circuits, Phys. Rev. X **13**, 041008 (2023).

[32] J. Yao and P. W. Claeys, Temporal entanglement barriers in dual-unitary clifford circuits with measurements, Phys. Rev. Res. **6**, 043077 (2024).

[33] L. H. Kauffman, *Knots and Physics*, 3rd ed. (WORLD SCIENTIFIC, 2001).

[34] See Supplemental Material for calculations for the Hopf link, algebra structure of gates, exact Renyi entropy and two-point correlation functions without meassurement, additional data for the effect of random replacements by swap gates and computation methods used in the paper.

COMPUTATION OF TOPOLOGICAL INVARIANT BY R MATRIX

The invariant of Hopf link is computed as

$$
\tau\left(\ \right) = \tau\left(\ \right)
$$
$$
+ \frac{2i}{\sqrt{1+c^2}}\ \tau\left(\ \right)
$$
$$
- \frac{2i}{\sqrt{1+c^2}}\ \tau\left(\ \right) \tag{15}
$$
$$
= n^2 + \frac{2i}{\sqrt{1+c^2}} k_- n - \frac{2i}{\sqrt{1+c^2}} k_+ n
$$
$$
= 4 + 2\frac{2i}{\sqrt{1+c^2}}\frac{2ic}{\sqrt{1+c^2}}
$$
$$
= \frac{4(c-1)^2}{1+c^2}
$$

In first equality we wrote a R as a sum of $R^\dagger$, I and P'. In second equality we used delooping relations in (17). This result shows our invariant is somewhat different from other invariant polynomials. It is proportional to the inner product $\langle\psi|P_{23}R_{12}R_{34}P_{23}|\psi\rangle$, where $|\psi\rangle$ is $\frac{1}{2}|\uparrow\uparrow + \downarrow\downarrow\rangle_{12}|\uparrow\uparrow + \downarrow\downarrow\rangle_{34}$, and the factor is $n^4 = 16$.

ALGEBRAIC RELATIONS OF R MATRIX

With the decomposition (5) and matrix representation (7) of R plus diagrammatic representations of R, P', I (4) and S (swap gate, (6)), it is straight forward to verify that they form an algebra. We denote X_i for the X element that acts on site i and $i+1$. First, P' alone is a Temperley-Lieb generator and if combined with S, which is a generator of symmetric group, then they are generators of a Brauer algebra as they satisfy

$$
S_i^2 = I_i,\ P_i'^2 = 2P_i'
$$
$$
[S_i, S_j] = [S_i, P_j'] = [P_i', P_j'] = 0 \text{ whenever } |i-j| > 1
$$
$$
S_i S_{i+1} S_i = S_{i+1} S_i S_{i+1},\ P_i' P_{i+1}' P_i' = P_i'
$$
$$
S_i S_{i\pm1} P_i' = P_{i\pm1}' P_i',\ P_i' S_{i\pm1} S_i = P_i' P_{i\pm1}'
$$
$$
S_i P_i' = P_i' S_i = P_i',\ P_i' S_{i\pm1} P_i' = P_i' .
\tag{16}
$$

Since swap gate is a special version of R ($|c| \to \infty$), it is natural to consider the algebra generated by R, P' and I. They generates the Birman–Murakami–Wenzl
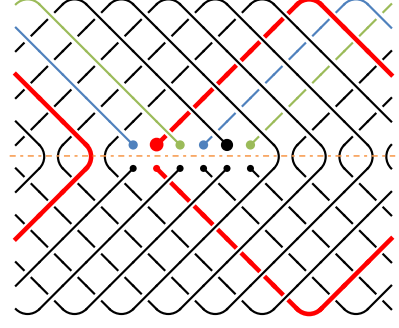

FIG. 5. (Color online) An example for the calculation of the second order Rényi entropy. The system length $L = 16$, the subsystem length $L_A = 6$ and the system evolves for 3 time steps. The 2 sites that connect to $\bar{A}$ are marked by larger dots and one of their worldlines is marked by a thickened red line. The horizontal dashed line separates the forward and backward evolution U and $U^\dagger$.

(BMW) algebra, as they satisfy (16) except that

$$
R_i^2 \neq I_i
$$
$$
R_j - R_j^\dagger = \frac{2i}{\sqrt{1+c^2}}\left(I_j - P_j'\right) \quad \text{(Skein relation)}
$$
$$
R_i P_i' = P_i' R_i = k_+ P_i' \quad \text{(Delooping relations)}
$$
$$
P_i' R_{i\pm1} P_i' = k_- P_i' \quad \text{(Delooping relations) (8)}
$$
$$
R_{\pm1} P_i' R_{\pm1} = R_i^\dagger P_{\pm1}' R_i^\dagger
$$
$$
R_{\pm1} P_i' P_{\pm1}' = R_i^\dagger P_{\pm1}',\ P_{\pm1}' P_i' R_{\pm1} = P_{\pm1}' R_i^\dagger
\tag{17}
$$

where $k_+ = e^{-i\theta}$, $k_- = e^{i\theta}$, $\theta = \arctan(c)$. This version of BMW algebra is not the original definition but modified to agrees with Kauffman's link invariant, and then it is isomorphic to Kauffman's tangle algebra. All the above can be easily checked using a diagrammatic representation or matrix multiplication. The circuit then is just an element of this algebra as it only involves the product of R, P' and I.

SOLVABLE CORRELATION AND EXACT RÉNYI ENTROPY WITHOUT MEASUREMENTS

Since our R matrix has graphical representation as a braid group generator, it is clearly dual-unitary. The advantage of dual-unitary gates is we can exactly compute the correlation functions. Moreover if we consider periodic boundary condition and the initial states are either infinite temperature state or tensor product of Bell states $\otimes (|\uparrow\rangle_i |\uparrow\rangle_{i'} + |\downarrow\rangle_i |\downarrow\rangle_{i'})$, then the exact Rényi entropy $S_n(t) = \frac{1}{1-n} \log_2 \text{Tr}\left(\rho_A^n(t)\right)$ of subsystem A is also known. For simplicity let us focus on the second order Rényi entropy. It equals to the number of sites that connect to the complement part $\bar{A}$. A simple example is shown in Fig. 5, where the initial state is the tensor
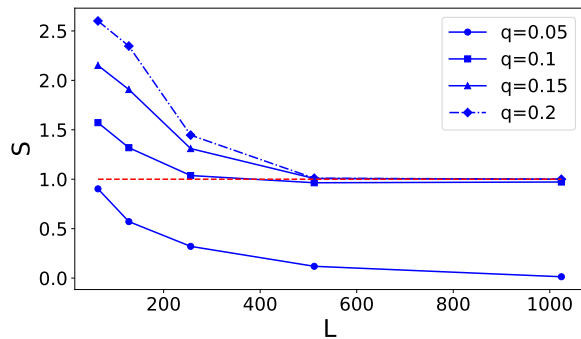
FIG. 6. Some data for points near phase boundary of CPLC at $p = 0.5$, $r = 0.1$ and $t = L$. When $q = 0.2$ the point is in critical phase and the other three are in area-law phase, but $q = 0.05$ shows different behavior as its entanglement approaches 0, since it is more far away from the transition boundary, compared to $q = 0.1, 0.15$. Red dashed line is a reference line for $S = 1$. All data points are averaged from 16384 samples.
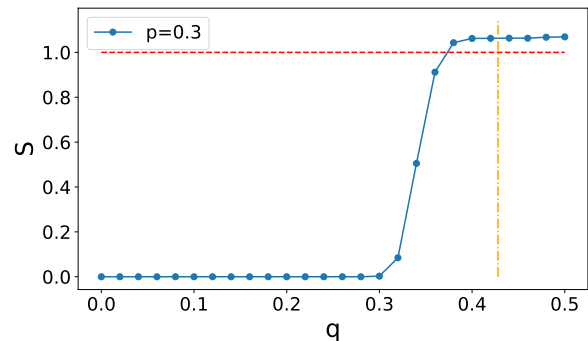

FIG. 7. Averaged entanglement for $p = 0.3$, $t = L = 512$. Red dashed line is a reference line for $S = 1$. Orange dash-dot line indicates the position of original transition point of CPLC. It is clear that under $r = 0.1$ replacement, the behavior of points near original phase boundary is different from their partners in area-law phase. All data points are averaged from 16384 samples.

product of 8 nearest-neighbor Bell states and the evolution time is 3. Since there are only 2 sites connecting to $\bar{A}$, $S_2 = 2$.

To see this, just note that there is no link between any two loops, which means we can separate them without cut. Thus $\mathrm{Tr}\left(\rho_A^2(t)\right) = 2^{\#(\mathrm{loops})-L}$, only depends on the number of loops formed by concatenating two replicas. If a site in A connects to $\bar{A}$, it will only contribute to one loop. So the overall Rényi entropy equals to the number of sites that connect to the complement part $\bar{A}$. Of course, if at some site R randomly flipped to $R^{\dagger}$, there will be links and the above number of sites gives an upper bound for Rényi entropy.

ADDITIONAL DATA AROUND PHASE BOUNDARIES

In this appendix we provide some additional data around phase boundaries, which shows evidence for suspected enriched phase or modified phase boundary at non-Clifford points. We set $r = 0.1$. As shown in Fig. 6, for data points near phase boundary of CPLC at $p = 0.5$ (the transition point is around 0.175), they converge to $S = 1$ (except for $q = 0.05$), but for $q = 0.2$, which is in critical phase, its entanglement is strictly larger than 1. The converged value of entanglement of $q = 0.1, 0.15$ is slightly less than 1. In contrast, when $q = 0.05$, or $p = 0.2$, $q = 0.2$ (not shown), the converged value is 0. We conjecture this is evidence for enriched phases or modified phase boundary at non-Clifford points. In Fig. 7, we plot the behavior of averaged entanglement at $p = 0.3$, $L = 512$. It shows additional entanglement acquired by points near critical phase, as stated in the main text.

COMPUTATION METHOD

For numerical simulation, we adopt a random sampling of trajectories and we average over all trajectories to get entanglement entropy. The probability for each gate to be either a R or P is independent from each other. This independence makes the direct simulation of the model feasible. In the following we introduce two methods we used for previous results.

Knitting and shuffling method for classical simulation

We use this method to simulate the circuit at Clifford points. In this case since each trajectory is only a pairing configuration plus worldline length distribution, it can be efficiently computed by updating a tableau similar to the stabilizer formalism. There are three kinds of continuous worldline with ends: 1. both ends are on final time boundary; 2. both ends are on initial time boundary; 3. two ends are on different boundary. The first two cases are pairings of sites and the third case contributes to the spanning number, which counts how many worldlines stretch through different time boundary and upper bounds the entanglement entropy of the TFDS. A pairing configuration of the state is a list of integer. The number a_i at site i stands for the pairings (i, a_i), that is site i connects to site a_i. For example, $(2,1,4,3)$ stands for the pairings $(1,2)$ and $(3,4)$. The length of worldline that starts from site i is recorded in a different list at site i. It is efficient to first prepare some stripes of size $(L, 2)$ and then recursively apply a knitting and shuffling method, which will reduce the total complexity to $L \ln L$, instead of L^2. This reduction works because the only important information is how boundaries are connected

and length distribution of worldlines, which we can easily read by moving a finger along worldlines. Every time we concatenate randomly two stripes to get a size-doubled stripe and record loops formed by this process. This operation takes $O(L)$ time. The total number of operation is $\ln L$, thus leading to a $O(L \ln L)$ time and space complexity (the number of loops is $O(L \ln L)$ because every concatenation produces at most $L/2$ loops).

Stabilizer method for Clifford cases

The circuit is Clifford when $c = 0, \pm 1$ and $|c| \to \infty$. In these cases we can use stabilizer to simulate the time evolution efficiently on a classical computer. The stabilizer method is $O(L^2)$ if we discard measurement results, so we cannot reach a system size as large as in knitting and shuffling method. But this method provides us a direct approach to exact entanglement. For projective measurements, we first project to XX, and project to ZZ forthwith. For $R(c = 1)$ gate, it is Clifford because it maps $X_1 \to -Y_1 Z_2$, $X_2 \to -Z_1 Y_2$, $Z_1 \to Y_1 X_2$, $Z_2 \to X_1 Y_2$.